Current understanding of jet noise-generation mechanisms from compressible large-eddy-simulations

Christophe Bailly[1] and Christophe Bogey[2]

[1] Laboratoire de Mécanique des Fluides et d'Acoustique
Ecole Centrale de Lyon & UMR CNRS 5509
69134 Ecully cedex, France
christophe.bailly@ec-lyon.fr
[2] Same address
christophe.bogey@ec-lyon.fr

Summary. In this paper, noise-generation mechanisms of subsonic round jets are investigated numerically. Compressible LES based on explicit filtering are carried out with the aim of computing directly aerodynamic noise. Both the aerodynamic and the acoustic fields are obtained for different Reynolds numbers. The LES procedure as well as comparisons of results with experimental data are described. Noise-generation mechanisms are then discussed in the light of simulations. Two noise contributions are identified, in agreement with the description of turbulent flows in terms of coherent structures and fine-scale turbulence.

1 Motivations

Prediction of the noise generated by a subsonic jet remains a difficult problem. One of the fundamental reason is the real complexity of the developing turbulent flow including the mixing between the jet exiting from a nozzle and the ambient medium. A numerical simulation must be capable, for instance, of relating subtle changes of the flow at the nozzle exit to the radiated noise with the aim of noise reduction. The involved noise-generation mechanisms, on the other hand, are not well understood and still debated in the recent literature.

Research efforts to identify noise sources have remained mostly theoretical and experimental. Theoretical approaches are generally based on overly simplifications of the turbulent jet flow, and measurements provide only a limited amount of information on the turbulence. A number of recent technical reviews of jet noise modelling [1, 2, 3, 4] are available. The present study focuses on the application of compressible large-eddy simulations (LES) to compute directly both the aerodynamic turbulent field and the correspond-

ing radiated acoustic field. With the direct noise computation (DNC), the investigation of sound-generation mechanisms takes the advantage that any turbulent quantity required for the analysis of the acoustic field is available. However, to have confidence in the DNC, serious numerical issues must be addressed before [5, 6]. LES enables to deal with more realistic jets and to study Reynolds number effects on the flow and its acoustics. Furthermore, the rapid development of computational aeroacoustics will allow us to take into account a part of the nozzle geometry in the simulation.

The present work is also motivated and guided by the following remarks. Turbulence and aerodynamic noise are intrinsically linked, and a direct identification of sound sources from only the radiated acoustic field is undoubtedly an intricate and ill-posed problem. In addition, methods for predicting the far-field noise from an accurate knowledge of the turbulent field or the near-pressure field are now well established. Before anything else, the challenge is to reproduce a high-fidelity DNC simulation of the flow including the thin turbulent shear layer of the exit boundary layer at the nozzle or the Reynolds-number effects for instance.

The present paper is organized as follows. In section 2, the numerical procedure used for the compressible LES is detailed. DNC results of round subsonic jets are presented in section 3 and compared with experimental data. Section 4 is devoted to the investigation of noise-generation mechanisms from the DNC data. Finally, concluding remarks are given in section 5.

2 Compressible LES based on an explicit filtering

Following the works of Vreman [7] *et al.*, the filtered compressible Navier-Stokes equations can be recasted as follows:

$$\begin{aligned} \partial_t \bar{\rho} + \partial_j(\bar{\rho}\tilde{u}_j) &= 0 \\ \partial_t(\bar{\rho}\tilde{u}_i) + \partial_j(\bar{\rho}\tilde{u}_i\tilde{u}_j + \bar{p}\delta_{ij} - \tilde{\tau}_{ij}) &= \sigma_i^{\text{sgs}} \\ \partial_t(\bar{\rho}\breve{e}_t) + \partial_j((\breve{e}_t + \bar{p})\tilde{u}_j + \tilde{q}_j - \tilde{\tau}_{ij}\tilde{u}_j) &= \sigma_e^{\text{sgs}} \end{aligned} \tag{1}$$

where ρ represents the density, u_i the velocity, p the pressure, τ_{ij} the viscous tensor and q_j the heat flux. The overbar denotes a filtered quantity, and the filtering is assumed to commute with the time and spatial derivatives. The tilde denotes the Favre (density-weighted) filtering $\tilde{u}_i = \overline{\rho u_i}/\bar{\rho}$. The variable $\breve{e}_t$ is defined as the total energy density of the filtered variables, *i.e.* $\bar{\rho}\breve{e}_t \equiv \bar{p}/(\gamma-1) + \bar{\rho}\tilde{u}_i\tilde{u}_i/2$ for a perfect gas, where γ is the specific heat ratio. The terms σ_i^{sgs} and σ_e^{sgs} in the right-hand side of (1) are the so-called subgrid-scale (SGS) terms. A detailed definition of each of the other terms of equation (1) is given in references [7, 8].

Low-pass filtering applied to any nonlinear problem introduces unknown terms which represent the interaction between the resolved scales and the non-resolved scales. Since the nineties, considerable efforts have led to clever

SGS models, see for instance the recent review of Meneveau and Katz [9], and to a better understanding of the interactions with the numerical algorithm solving the governing equations. In parallel, several studies have also pointed out some difficulties to reproduce correctly the behavior of high-Reynolds number flows [10] or of transitional shear flows [11, 12]. This is especially the case when the SGS model is based on a turbulent viscosity which has the same functional form as the molecular viscosity.

An alternative to the modelling of the SGS terms is to recover the unfiltered variables appearing in the SGS terms. These deconvolution or more generally defiltering procedures are used to directly compute the SGS terms involving nonlinear interaction between the scales supported by the numerical grid but not accurately resolved by the algorithm. However, the energy transfert between the resolved and the non-resolved scales of the grid need also to be modelled. In the Approximate Deconvolution Model (ADM) introduced by Stolz [13] *et al.* for instance, a relaxation term draining the energy to non-resolved scales is introduced in the equations to take into account the scales not represented by the numerical grid, and thus to provide a sufficient SGS dissipation. A review of these approaches has been written by Domaradzki and Adams [14].

A highly accurate algorithm has been developed in our works for solving the compressible Navier-Stokes equations [8, 15, 16] in this framework, but also to perform a direct computation of the noise generated by turbulent flows. The discretization of the governing equations is performed with an optimized thirteen-point stencil finite-difference scheme for the spatial derivation. The modified wavenumber of the scheme is plotted in figure 1 for a uniform mesh of grid spacing Δx. Wavenumbers $k\Delta x \leq k_c^s \simeq 1.83$ are accurately discretized without significant dispersion [15]. The cutoff or Nyquist wavenumber of the grid is given by $k_c^g \Delta x = \pi$, and the corresponding grid-to-grid oscillations are not resolved. They are removed by a high-selective filtering, which is also used as to model the dissipative effects of the SGS. The filter coefficients have been optimized in the Fourier space [15]. The first kth moments of G are zero ($1 \leq k \leq 3$) among the different properties of this class of filters [17]. The transfer function $\hat{G}$ of the filter is shown in figure 2. Wavenumbers such that $k\Delta x \leq k_c^f \Delta x = \pi/2$ are not affected by the filtering, and are also well represented by the numerical grid. As shown in the same figure 2, the present filter is very close to the secondary filter proposed by Stolz [12, 13] and coworkers in the ADM. The different scales involved in the numerical resolution are collected in figure 3.

To summarize, the following equations are therefore solved in the present LES procedure:

$$\partial_t \mathbf{U} + \nabla.\mathbf{F}(\mathbf{U}) = -(\sigma_d/\Delta t)(1 - G) * (\mathbf{U} - \langle \mathbf{U} \rangle)$$

where $\mathbf{U} = (\bar{\rho}, \bar{\rho}\tilde{\mathbf{u}}, \bar{\rho}\breve{e}_t)$, the vector $\mathbf{F}$ is given by the left-hand side of (1), and $\langle \cdot \rangle$ represents a statistical averaging. All the non-linear terms are computed from the filtered quantities as for a no-model procedure [12, 19, 20]. Note

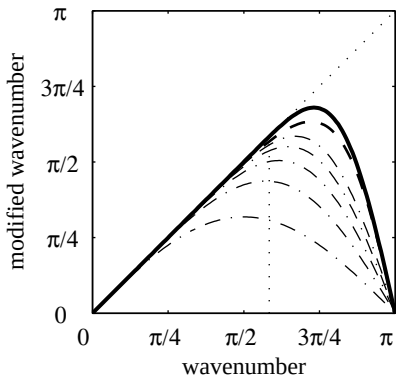

Fig. 1. Plot of modified or effective wavenumber of the scheme versus exact wavenumber: optimized 13-points finite difference scheme of Bogey and Bailly [15] ——— , 6th-order compact scheme of Lele [18] - - - and 2nd, 4th, 6th, 8th and 10th-order central differences –·–·– . Wavenumbers up to $k\Delta x \simeq 1.83$ or $\lambda/\Delta x \geq 3.5$ are accurately resolved by the 13-pts optimized scheme.

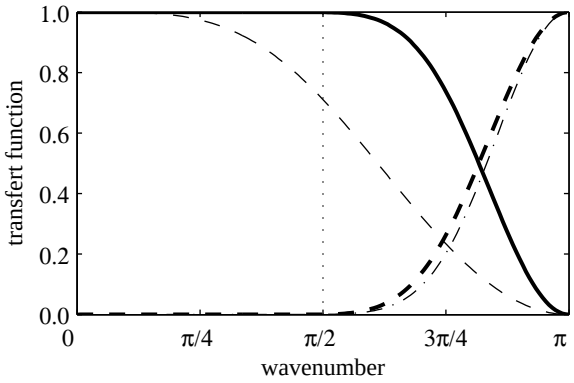

Fig. 2. Transfer function of the optimized 13-points filter of Bogey and Bailly [15] $\hat{G}$ ——— , and of $\hat{D} = 1 - \hat{G}$ - - - . The tranfer functions involved in the approximate deconvolution model [12] are also plotted : – – – implicit primary filter $\hat{G}_i$, and –·–·– secondary filter $\hat{H}_N = 1 - \hat{Q}_N \cdot \hat{G}_i$ ($N = 5$ and $k_c\Delta x = 1/2$).

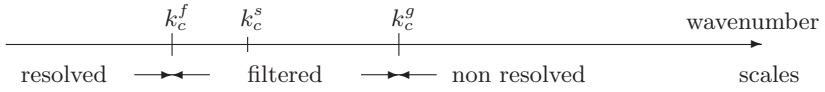

Fig. 3. Scales involved in the numerical algorithm for LES. The cutoff frequency of the grid is given by $k_c^g \Delta x = \pi$ but only the scales $k \leq k_c^f$ are accurately resolved. The scales with $k_c^f < k < k_c^g$ are filtered. Note that the accuracy limit of the spatial numerical derivation is such that $k_c^s \geq k_c^f$.

also that the independence of the results from the filtering has been studied recently [21]. A six-stage low-storage Runge-Kutta algorithm [15] ensures the time integration. Specific non-reflecting boundary conditions are implemented to preserve the acoustic field generated by the turbulent flow. For further details concerning the implementation of the filtering and of the boundary conditions, the reader is referred to [8, 15].

3 Direct noise computation of round subsonic jets

The feasibility of the direct computation of noise via compressible LES was demonstrated by Bogey & Bailly [22] for a jet at near sonic conditions, with successful comparisons between predictions and measurements for the flow and for the acoustic. This earlier work was based on the Smagorinsky SGS model.

All the results reported subsequently are obtained with the LES procedure described in section 2, with focus on isothermal jets at Mach number $\mathrm{M} = u_j/c_\infty = 0.9$ and at different Reynolds numbers $\mathrm{Re}_D = u_j D/\nu$ where u_j is the jet exit velocity, $D = 2r_0$ the jet diameter, ν the kinematic viscosity and c_∞ the ambient speed of sound. The mean velocity profile at the inflow is defined by a hyperbolic-tangent profile with a ratio between the shear-layer momentum thickness and the jet radius of $\delta_\theta/D = 2.5 \times 10^{-2}$. Small random vortical perturbations are added to the mean velocity profile in the initial shear-layer zone to seed the turbulence [8, 22]. The influence of these inflow conditions on the flow development as well as on the sound field is investigated in a recent paper [16]. The computational domain is discretized by a 12.5 million point Cartesian grid with 15 points in the jet radius. The flow is calculated up to $25r_0$ in the axial direction, and up to $15r_0$ in the transverse directions including a portion of the radiated sound field. Sound waves are accurately resolved up to a Strouhal number $\mathrm{St} = fD/u_j \leq 2$.

Snapshots of jets for Reynolds numbers varying from $\mathrm{Re}_D = 1.7 \times 10^3$ to 4×10^5 are presented in figure 4. These pictures clearly show the strong modification of the radiated pressure, with the emergence of high-frequency waves in the sound field at 90° to the jet axis as Re_D is increased. For the lowest Reynolds number, the radiation pattern seems very similar to the radiation of instability waves in supersonic flows. The same behaviors have been observed for Mach number $\mathrm{M} = 0.6$ jets [23]. The influence of the Reynolds number is also clearly visible on the turbulent flow itself with a larger range of vortical scales when the Reynolds number increases. The ratio δ_θ/D being kept constant in all the simulations, the decrease of the initial momentum thickness δ_θ with Re_D leads to a stronger viscous diffusion and a larger length of the potential core, from $x_c \simeq 5D$ to $7D$. For $\mathrm{Re}_D = 1.7 \times 10^3$, the development of the turbulent flow occurs even notably later downstream, which prevents vortex pairing.

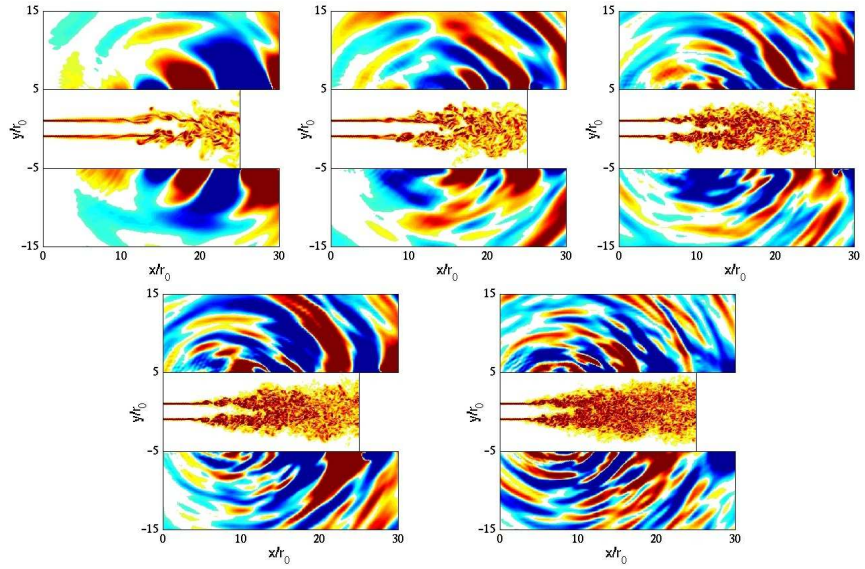

Fig. 4. Jets at Mach number M = 0.9. Snapshots of the vorticity norm in the flow and of the fluctuating pressure outside, in the plane $z = 0$, for Reynolds number $\mathrm{Re}_D = 1.7 \times 10^3, 2.5 \times 10^3, 5 \times 10^3, 1 \times 10^4$ and 4×10^5. The pressure color scale is $[-70, 70]$ Pa for all the simulations.

Figure 5 shows the evolution of the mean axial velocity u_c/u_j in the downstream direction for different Reynolds numbers. A good agreement is observed between numerical results and experimental data. The mean velocity decay is more rapid for low Reynolds-number flows. Axial profiles of the turbulence intensity u'_{rms}/u'_j are also reported. For low Reynolds numbers, transition to turbulence occurs later as mentioned before. Moreover, turbulence intensity reach higher values in agreement with measurements. All these effects are accurately reproduced with the present LES procedure [11, 23].

4 Jet noise mechanisms

The understanding of aerodynamic noise is intrinsically linked to the description of the turbulence. Turbulent flows contain a broad range of scales which generally belong to one of the two following classes. The first one consists of fine-scale turbulence, associated with random motions in turbulent flows, and ranged in size from the larger scale given by the size of the flow, *i.e.* the nozzle diameter for a jet, to the smallest one, namely the Kolmogorov scale l_η. The other class contains coherent structures or wave-packets. These large scales dominate the flow, are organized, and are often reminiscent of instability waves. To avoid some confusions, note that large scales in LES contain

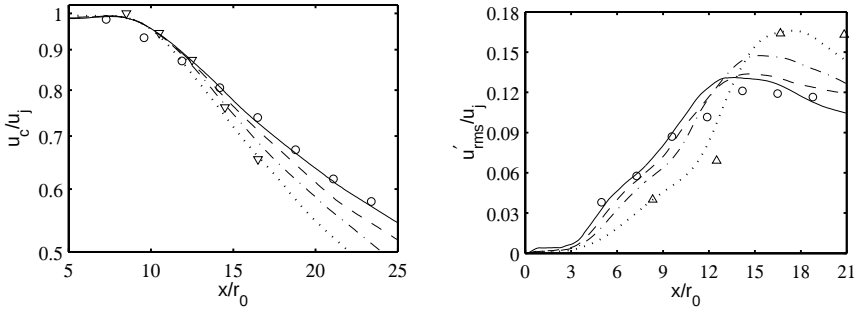

Fig. 5. Jets at Mach number M = 0.9. Left, axial profile of the mean velocity u_c/u_j, and right, axial profile of the rms fluctuating axial velocity $u'_{\rm rms}/u_j$. Simulations: —— $\mathrm{Re}_D = 4\times10^5$, – – – $\mathrm{Re}_D = 10^4$, –·–· $\mathrm{Re}_D = 5\times10^3$ and ····· $\mathrm{Re}_D = 2.5\times10^3$. Measurements: ▽ Stromberg [24] *et al.* (M = 0.9, $\mathrm{Re}_D = 3.6\times10^3$), ○ Arakeri [25] *et al.* (M = 0.9, $\mathrm{Re}_D = 5\times10^5$). △ DNS of Freund [26] (M = 0.9, $\mathrm{Re}_D = 3.6\times10^3$). Note that all the profiles are shifted in the axial direction to display the same potential core length.

both fine-scale turbulence and coherent structures. Large scales in this context mean scales resolved by the computational grid, and not only coherent structures.

From an experimental point of view, most of the noise originates from near the end of the potential core [27], and seems to be associated with the breakdown of the coherent structures [28]. Two-point azimuthal correlations of the acoustic pressure display high levels in the main emission direction at shallow angles [29, 30]. Lower correlation-levels are measured for angles $\theta \simeq 90^{\rm o}$ from the jet axis and they appear enhanced as Re_D decreases. In the classical framework, this change of the acoustic field with the angle is attributed to mean flow effects on sound propagation [31].

The present numerical works bring support to the conjecture of two distinct noise components as proposed by Tam [32]. The structure of the sound fields have been investigated numerically [23] for the two observation positions $\theta \simeq 30^{\rm o}$ and $\theta \simeq 90^{\rm o}$, and two acoustic radiations have been identified:

- a component nearly independent from the Reynolds number, which dominates the sound field in the downstream direction with a low-frequency spectrum, and high levels of azimuthal correlation. A Strouhal scaling is observed for the spectral peak with a u_j^9 power law. The noise mechanism involved appears to be linked to the periodic intrusion of vortical coherent structures into the jet [22].
- a component closely dependent on the Reynolds number, which vanishes as Re_D decreases. A Strouhal scaling is found for this broadband acoustic radiation, with a weak azimuthal correlation, and a $u_j^{7.5}$ power law. This component is responsible for the noise emitted in the sideline direction at high-Reynolds number whereas its contribution at lower angles is masked

by the previous component. It is mainly generated by the transional flow in the shear-layer developping from the nozzle exit to the end of the potential core, and is therefore direcly connected to Re_D.

Among the different results obtained, the scaling of the peak of the acoustic spectra in the downstream and sideline directions versus the Reynolds number is reported in figure 6. The two noise contributions are distinguished with a fairly constant Strouhal number for the first one, and a Strouhal number decreasing at lower Reynolds numbers for the second one.

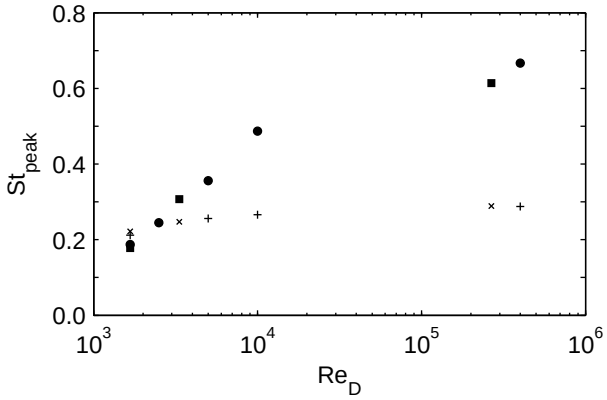

Fig. 6. Peak Strouhal number versus Reynolds number obtained for the + Mach 0.9 and × Mach 0.6 jets in the downstream direction $\theta \simeq 30^{\circ}$, and for • Mach 0.9 and ■ Mach 0.6 in the sideline direction, $\theta \simeq 90^{\circ}$.

Noise-source mechanisms can be identified by establishing direct links between turbulent flow events and emitted sound waves. In particular, the causality method can be applied to LES data [33] by calculating the following normalized cross-correlation function:

$$C_{fp}\left(\boldsymbol{x}_1, \boldsymbol{x}_2, t\right) = \frac{\left\langle f(\boldsymbol{x}_1, t_0)\, p'(\boldsymbol{x}_2, t_0 + t)\right\rangle}{\left\langle f^2(\boldsymbol{x}_1, t_0)\right\rangle^{1/2} \left\langle p'^2(\boldsymbol{x}_2, t_0)\right\rangle^{1/2}}$$

between two points $\boldsymbol{x}_1$ and $\boldsymbol{x}_2$, at two times seperated by t. A review from the experimental point of view can be found in reference [34]. Since all the turbulent quantities are available in simulations, variables such as $f = u', v', w', u'u', v'v', w'w'$, k (kinetic energy) or ω (norm of the vorticity vector) can be correlated to the acoustic pressure p'. As an illustration, figure 7 shows the correlation obtained between the centerline vorticity and the pressure signal at $\theta = 40^{\circ}$. A significant correlation level is found near the end of the potential core, and this result still holds when the Reynolds number varies [33], which corroborates the presence of the coherent-noise component. In the same way, the correlations between the flow, along the shear-layer as

well as along the jet axis, with the acoustic pressure are found to be very weak or insignificant.

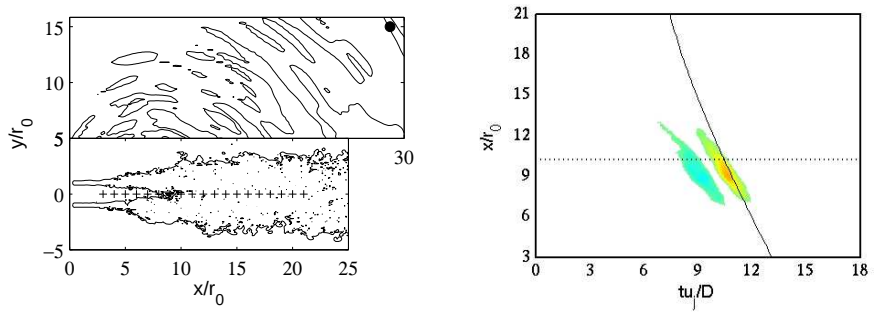

Fig. 7. Identification of noise sources by cross-correlations between vorticity along the jet axis and pressure at the point •, located at $\theta = 40^{\circ}$ in the acoustic field for the $\mathrm{Re}_D = 4 \times 10^5$ jet. The color scale is defined from -0.14 to 0.14, with white in the range [-0.035 0.035]. The solid line represents the acoustic propagation time between the centerline points + and the observer point •. The dotted line shows the end of the potential core.

5 Perspectives

The present direct noise computations, based on compressible LES with explicit filtering, support the presence of two distinct jet noise-generation mechanisms, corresponding to a decomposition of the turbulent field into coherent structures and fine-scale turbulence. These two noise contributions have specific characteristics which can be identified. In particular, the Reynolds number dependence is well reproduced by the LES for the sound field in the sideline direction. One of the next step is to include a part of the nozzle to better simulate the incoming transitional turbulent flow. This work is in progress and should allow to study noise reduction concepts involving chevrons or beveled nozzles.

Acknowledgments

The first author is grateful to the organizers of the DLES-6 for their invitation to present this talk. Computing time and technical assistance provided by the Institut du Développement et des Ressources en Informatique Scientifique (IDRIS - CNRS) are deeply appreciated.

References

1. Huff, D. (compiler) (2001) Proceedings of the jet noise workshop, CP-2002-211152, 1071 pages, [www http://gltrs.grc.nasa.gov/]
2. Morris P.J. & Farassat F. (2002) *AIAA Journal* 40(4):671–680.
3. Bailly C., Bogey, C. (2004) *Int. J. Comput. Fluid Dynamics* 18(6):481–491.
4. Lele S. (2005) In proceedings of Turbulence and Shear Flow Phenomena-4, Williamsburg, VA, USA, 27-29 june, (3):889–898
5. Tam C.K.W. (1995) *AIAA Journal* 33(10):1788–1796.
6. Lele S.K. (1997) *AIAA Paper* 97-0018.
7. Vreman B., Geurts B., Kuerten H. (1995) *Applied Scientific Research* 54:191–203.
8. Bogey C., Bailly C. (2005) *Computers and Fluids* in press :1–15.
9. Meneveau C., Katz J. (2000) *Annu. Rev. Fluid Mech.* 32:1–32.
10. Porter D.H., Woodwrad P.R., Pouquet A. (1998) *Phys. Fluids* 10(1):237–245.
11. Bogey C., Bailly C. (2005) *AIAA Journal*, 43(2):437–439.
12. Schlatter P., Stolz S., Kleiser L. (2004) *Int. J. Heat and Fluid Flow* 25:549–558.
13. Stolz S., Adams N.A., Kleiser L. (2001) *Phys. Fluids* 13(4):997–1015.
14. Domaradzki J.A., Adams N.A. (2002) *Journal of Turbulence* 3(024):1–19.
15. Bogey C., Bailly C. (2004) *J. Comput. Phys.* 194(1):194–214
16. Bogey C., Bailly C. (2005) *AIAA Journal* 43(5):1000–1007.
17. Vasilyev O.V., Lund T.S., Moin P. (1998) *J. Comput. Phys.* 146:82–104.
18. Lele S.K. (1992) *J. Comput. Physics* 103(1):16–42.
19. Rizzetta D.P., Visbal M.R., Blaisdell G.A. (2003) *Int. J. Numer. Meth. Fluids* 42:665–693.
20. Mathew J., Lechner R., Foysi H., Sesterhenn J., Friedrich R. (2003) *Phys. Fluids* 15(8):2279–2289
21. Bogey C., Bailly C. (2005) In proceedings of Turbulence and Shear Flow Phenomena-4, Williamsburg, VA, USA, 27-29 june, (2):817–822, accepted in the *International Journal of Heat and Fluid Flow*.
22. Bogey C., Bailly C., Juvé D. (2003) *Theoret. Comput. Fluid Dynamics* 16(4):273–297.
23. Bogey C., Bailly C. (2004) *AIAA Paper* 2004-3023:1–15.
24. Stromberg J.L., McLaughlin D.K., Troutt, T.R. (1980) *J. Sound Vib.* 72(2):159–176.
25. Arakeri V.H., Krothapalli A., Siddavaram V., Alkistar M.B., Lourenco L.(2003) *J. Fluid Mech.* 490:75–98.
26. Freund J.B. (2001) *J. Fluid Mech.*, 438:277–305.
27. Juvé D., Sunyach M., Comte-Bellot G. (1980) *J. Sound Vib.* 71(3):319–332.
28. Hussain A.K.M.F. (1986) *J. Fluid Mech.* 173:303–356.
29. Maestrello L. (1976) *NASA* TMX-72835.
30. Juvé D., Sunyach, M. (1978) *C. R. Acad. Sci. Paris*, B, 287:187–190.
31. Goldstein M.E., Leib S.J. (2005) *Journal Fluid Mech.* 525:37–72.
32. Tam C.K.W. (1998) *Theoret. Comput. Fluid Dynamics* 10:393–405.
33. Bogey C., Bailly C. (2005) *AIAA Paper* 2005-2885:1–18.
34. Panda J. (2005) *AIAA Paper* 2005-2844.